University of Bath

Efficient Hematite Photoanodes Prepared by Hydrochloric Acid-treated Solutions with Amphiphilic Graft Copolymer

Min Su Park,[a] Dominic Walsh,[b] Jifang Zhang,[b] Jong Hak Kim[a,*] and Salvador Eslava[b,*]

[a] *Department of Chemical and Biomolecular Engineering, Yonsei University, 50 Yonsei-ro, Seodaemun-gu, Seoul 120-749, South Korea*

[b] *Department of Chemical Engineering, University of Bath, Bath BA2 7AY, United Kingdom*

[*] To whom correspondence should be addressed:

Prof. Jong Hak Kim E-mail: jonghak@yonsei.ac.kr

Dr. Salvador Eslava E-mail: S.Eslava@bath.ac.uk

Abstract

Simple and low-cost approaches for the preparation of photoelectrodes are crucial to enable a transition towards a sustainable and circular economy in which sunlight energy is efficiently harnessed and used. Here, a novel and simple process is presented to prepare a sol solution that can be cast by spin coating deposition for mesoporous α-Fe$_2$O$_3$ hematite water-splitting photoanodes, reaching 1.05 mA cm^{-2} at 1.23 V$_{RHE}$ under 1 sun illumination. The sol solution is prepared using inexpensive commercial ~10 nm α-Fe$_2$O$_3$ hematite nanoparticles as hematite film precursor, an amphiphilic poly(vinyl chloride)-*graft*-poly(oxyethylene methacrylate) (PVC-*g*-POEM) graft copolymer as a pore template, and HCl acid as an iron oxide phase directing agent. The hydrophilic POEM side chains selectively interact with HCl-treated hematite nanoparticles allowing their dispersion. Moreover, the HCl in the sol solution disperses and dissolves the hematite nanoparticles which re-precipitate as mixed phase γ-FeOOH and β-FeOOH, leading to better performant hematite films due to finer nanostructures, a more pronounced hematite (110) plane, and a more hydroxylated surface. This work demonstrates that synergies between an amphiphilic graft copolymer, hematite nanoparticles and HCl acid can be exploited in the inexpensive spin coating technique to prepare robust, stable and promising hematite photoanodes for energy devices.

Keywords: graft copolymer; mesoporous hematite; photoanode; photocatalyst; solar water splitting.

1. Introduction

The world's energy demands continue to increase owing to population growth and economic expansion of India and China among other major countries. However, traditional fossil fuels have limitations such as air pollution and climate effects due to contaminants or greenhouse gases, which in turn adversely affect the Earth's ecosystem. Thus, interest in utilizing solar energy has increased markedly [1,2]. A photoelectrochemical (PEC) cell has the potential to produce hydrogen and oxygen from water using solar energy without the emission of contaminants. TiO_2 [3-5], ZnO [6], α-Fe_2O_3 (hematite) [7-10] and WO_3 [11-13] are commonly reported metal oxide semiconductors employed as a photoanode absorbing layer in PEC cells. Among them, hematite has been widely studied as one of the prospective photoanode materials since it has an optimal band gap for visible light absorption (1.8 - 2.2 eV), remarkable chemical stability for oxidation [14], very low cost and toxicity and high abundance [15-19].

Hematite has excellent properties but also drawbacks for application at an industrial scale, specifically it possesses low penetrating ability of photons at visible wavelengths [20], high tendency to recombine electrons and holes [21,22], poor charge carrier mobility and short hole diffusion length (2-20 nm) [23,24]. These drawbacks are mitigated by different approaches, such as fabricating intricate structures [7,25-27] and promoting the (110) hematite crystalline plane over the (104) plane [28], both to optimize the electron pathway. However, these approaches often have no scale-up capability or are too complicated and expensive. It is therefore necessary to find facile and inexpensive methods to nanostructure hematite and promote (110) hematite crystalline plane.

TiO_2 [29,30], SnO_2 [31], TiN [32] and even $MgTiO_3$ perovskite [33] have been fabricated using amphiphilic copolymers, which consist of combined hydrophilic and hydrophobic chains. These polymers are usually categorized as two forms of structural directing agents; block

copolymers and graft copolymers. It is known that graft copolymers are potentially more viable in comparison to conventional block copolymers, due to their more economical and facile synthetic route [34]. The use of a block copolymer as a structural directing agent for hematite has been previously reported but it only achieved a few μA cm^{-2} at 1.23 V$_{RHE}$ [26]. The use of graft copolymers on hematite photoanodes remains unexplored to the best of our knowledge.

Here we report for the first time the fabrication of inexpensive mesoporous hematite films via spin coating a sol solution prepared with commercial hematite nanoparticles, a (poly(vinyl chloride)-*graft*-poly(oxyethylene methyl ether methacrylate) PVC-*g*-POEM amphiphilic graft copolymer, and HCl acid, achieving photocurrents of 1 mA cm^{-2} at 1.23 V$_{RHE}$, competitive values for a solution process with scale-up capability. These hematite films show wormlike mesoporosity with particles down to 67 ± 19 nm, predominance of the (110) plane over the (104) one, and a passivated surface full of hydroxyl groups. Partial dissolution of hematite particles into FeOOH sol solutions is shown crucial in optimizing final properties and performance.

2. Experimental Section

2.1. Polymer Synthesis

PVC (average Mw ~ 233,000, and average Mw ~ 80,000), POEM (average Mn 500, containing 100 ppm of hydroquinone monomethyl ether MEHQ and 200 ppm of butylated hydroxytoluene BHT as inhibitors), HMTETA (97 %), and copper(I) chloride (CuCl(I), ReagentPlus®, purified, $\geq$ 99 %) were all supplied by Sigma-Aldrich. Methanol (HPLC grade) was supplied by Daejung Chemicals and Metals Co. Ltd.

First, 6 g of PVC was dissolved homogeneously in 50 mL of n-methyl-2-pyrrolidone (NMP) in a round-bottom flask at 50 °C. Subsequently, 0.1 g of CuCl(I) and 0.624 mL of HMTETA were

added to the flask. After 6 mL of POEM was added, the solution was N_2 purged for 30 min. Finally, the homogenous green solution was held at 90 °C for 24 h. The synthesized graft copolymer was precipitated in 400 mL of methanol and washed three times in this volume of methanol for 9 h soaking time. The resultant polymer was dried at 50 °C overnight.

2.2 Fabrication of hematite photoanodes

Sicotrans® Red L 2715 D (α-Fe$_2$O$_3$) hematite nanoparticles (ca. 10 nm diameter) was supplied by BASF. HCl (37% in water) and THF were purchased from VWR chemicals. 2-Propanol (IPA, 99+ %) and 1-hexanol (99 %) were purchased from Alfa Aesar. ABS glass (P-LZ-00, Solaronix SA, Switzerland) coated on one face with FTO were cut into rectangular 12 mm x 25 mm pieces and used as a substrate for preparing hematite photoanodes. Acac-treated hematite precursor was prepared by modification of a previous reported procedure [7]. Briefly, 0.1 mL of mixture of 0.04 mL of acac and 0.477 mL of 1-hexanol were added to 0.4 g of BASF Sicotrans® Red L 2715. The mixture was stirred with gradual addition of 4.48 mL of IPA before sonication for 5 min followed by stirring for 10 min before drying at 40 °C. To prepare hematite photoanodes on ABS-FTO glass substrates, 0.1 g of PVC-*g*-POEM was dissolved in 1.76 mL (6 wt%) of THF at 50 °C. 30 mg of the prepared acac-hematite precursor were dispersed in the prepared homogeneous THF-copolymer solutions by ultra-sonication for 10 min. 0, 0.05, 0.1 or 0.15 mL of 37 wt% HCl was then added and the resulting mixtures stirred overnight. All prepared resulting sol solutions were cast by spin-coating onto the ABS-FTO glass pieces using 1000 rpm for 20 sec and dried for 1 hour to remove solvents. The heating process consisted of three steps, firstly the coated glass samples were heated to 200 °C at 3.8 °C/min rate and held for 20 min to remove residual solvent. Secondly, the samples were calcined to 500 °C at 3.8 °C/min rate and held for 20 min to sinter the films and eliminate the copolymer.

Finally, photoanodes were suddenly heated to 800 °C in air for 20 min to induce tin migration into the hematite coatings [7].

2.3 Characterization

FT-IR (Spectrum 100, PerkinElmer) was utilized to characterize the copolymer. NMR (500 MHz Bruker Avance II+) spectra also confirmed the rough ratio of PVC main chains and POEM side chains in the synthesized copolymer. FE-SEM (JEOL-6301F) was employed to observe the morphology of photoanode surfaces and cross-sections. No conductive coating was deposited. SEM surface micrographs were analyzed for particle size and surface coverage with ImageJ software. Particles in sol solutions were observed by TEM (JEOL 2100 Plus). Solutions were diluted in THF followed by sonication for 10 min before a drop was dried onto carbon coated copper TEM grids. XPS spectra of electrode surfaces were measured by X-ray photoelectron spectroscopy (K-alpha, Thermo U. K.). Light absorption of photoanodes was measured by UV-Vis spectroscopy (CARY 100). XRD patterns of powder samples were measured on a BRUKER D8-Advance (Cu radiation).

2.4 Photoelectrochemical performance

Photocurrent density and IPCE were investigated in a three-electrode photoelectrochemical quartz cell. Simulated sun light on an 0.283 cm^2 area was supplied by a 300 W Xe Lamp (LOT Quantum Design) using a AM 1.5G filter (which simulates the terrestrial solar spectrum at ground level). The illumination intensity was set to 1 sun (100 mW cm^{-2}). In the three electrode system, the working electrode was the as-prepared hematite photoanode, the counter electrode was a Pt wire, and an Ag/AgCl (in 3.5 M KCl) electrode was the reference electrode. 1 M KOH solution (pH 13.85) was used as an electrolyte. Photocurrent density-potential (j-V) curves were recorded at a scan rate of 20

mV s^{-1}. The measured potentials vs. Ag/AgCl (E$_{Ag/AgCl}$) were converted to RHE potential (E$^{\circ}_{RHE}$) following the Nernst equation:

$$E^{\circ}_{RHE} = E^{\circ}_{Ag/AgCl} + E_{Ag/AgCl} + 0.059 \text{ pH} \qquad (1)$$

The IPCE values were calculated using the following equation:

$$\text{IPCE} (\lambda) = \{|j \text{ (mA cm}^{-2})| \cdot 1239.8 \text{ (V nm)}\} / \{P_{mono} \text{ (mW cm}^{-2}) \cdot \lambda \text{ (nm)}\} \qquad (2)$$

where j is the photocurrent density under the designated wavelength (λ) light illumination and P$_{mono}$ is the power of the incident irradiation.

The ± symbol next to mean values denotes standard deviation.

3. Result and discussion

3.1 Amphiphilic graft copolymer (PVC-g-POEM) synthesis
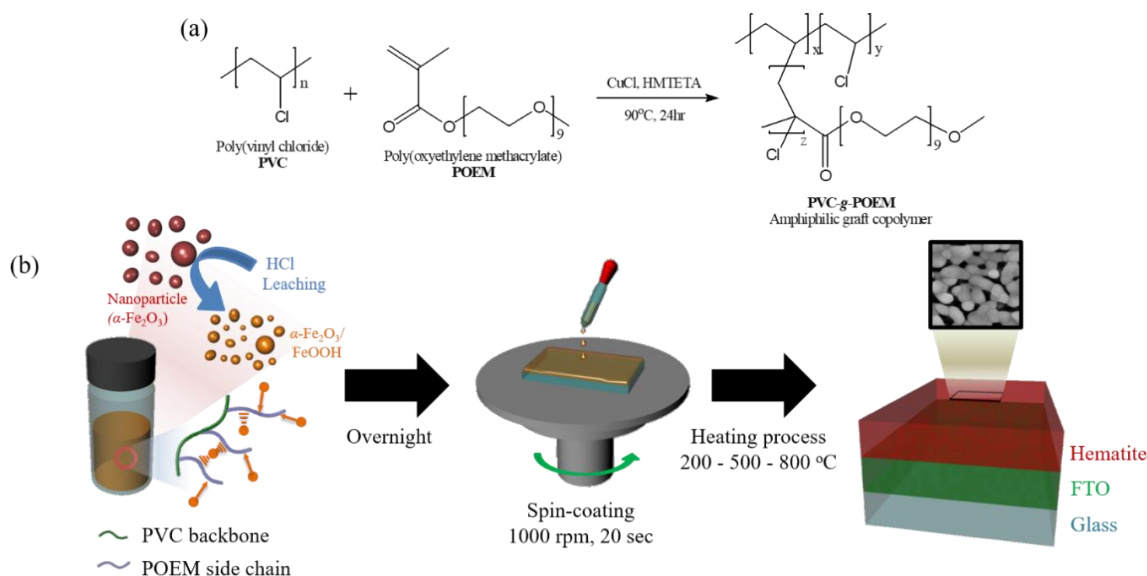
Scheme 1. Schematic diagrams of (a) the synthesis of PVC-*g*-POEM amphiphilic graft copolymer and (b) the fabrication of mesoporous hematite photoanodes

Amphiphilic graft copolymer PVC-g-POEM was prepared in N-methyl-2-pyrrolidone (NMP) using commercially available PVC homopolymer and POEM macromonomer, CuCl(I) catalyst and hexamethyltriethylenetetramine (HMTETA) ligand in nitrogen atmosphere at 90 ℃ for 24 h (Scheme 1). Next, it was precipitated and washed with methanol and dried at 50 °C overnight. Prepared PVC-*g*-POEM gave characteristic IR absorbance of both PVC main chains (C-Cl, 608 cm^{-1}) and POEM side chains (C=O, 1728 cm^{-1}, C-O, 1096 cm^{-1}) (Figure S1). In particular, the C=C (1637 cm^{-1}) absorbance present in POEM macromonomer is not present in PVC-*g*-POEM, indicating that POEM side chains are well-attached to PVC main chains as well as the clear elimination of unreacted POEM due to repeated solvent washing. Moreover, the ester C=O absorbance is shifted from 1717 to 1728 cm^{-1} and ether C-O absorbance from 1110 to 1096 cm^{-1}. This is consistent with restriction of the ester group by grafting and dipole interaction through weaker bond energy. Overall, FT-IR shows that the hydrophilic rubbery POEM macromonomer was successfully grafted to hydrophobic glassy PVC main chains.

Grafting ratio of POEM side chains to PVC main chains was confirmed by ^{1}H nuclear magnetic resonance (NMR, 500 MHz, THF-d$_8$, Figure S2). Broad signals around 4.3-4.7 (H; -CHCl-), 2.0-2.4 ppm (2H; -CH$_2$-) correspond to the hydrogen in PVC main chains. Moreover, 4.1 (2H; -COO-CH$_2$-), 3.4-3.8 (2H; -CO-CH$_2$-) and 3.3 ppm (3H; -CO-CH$_3$) signals were detected for POEM side chains. The molar grafting ratio of POEM is calculated to be 6.1 % in the total copolymer by considering the area of each characteristic peak. In terms of weight ratio, approximately 35 wt.% of POEM macromonomer were covalently attached as side chains. Based on the known molecular weight of the PVC the M$_n$ and M$_w$ of the PVC-*g*-POEM graft copolymer were 150 and 343 KDa, respectively.

3.2 Photoanodes preparation and optimization

PVC-*g*-POEM graft copolymer in various amounts was dissolved in tetrahydrofuran (THF) and mixed with ~10 nm α-Fe_2O_3 nanoparticles coated with acetylacetone (acac). These hematite nanoparticles are inexpensive, since they are commercialized in large scale as a red pigment for the painting industry. Different small amounts of concentrated aqueous HCl were then added and the resulting mixtures stirred overnight. All prepared sol solutions were cast by spin-coating onto fluorine-doped tin oxide (FTO) coated aluminoborosilicate (ABS) glass. Finally, coated glass samples were annealed in air at 200, 500 and 800 °C for organic decomposition and porous film formation (Scheme 1).
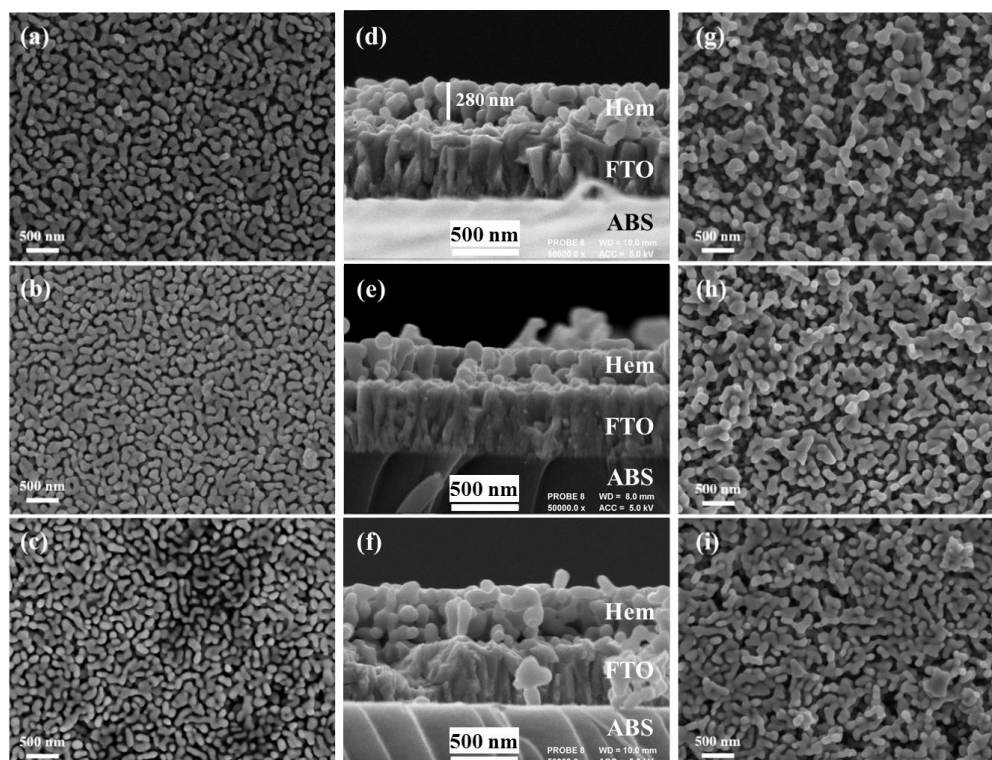
Figure 1. (a-c) Surface and (d-e) cross-sectional SEM micrographs of hematite photoanodes prepared with either (a,d) one, (b,e) two or (c,f) three layers. Calcination and sintering was done after each layer deposition. Spin coating precursor sol solution were prepared with 0.1 ml of 37% HCl. (g-i) Surface SEM micrographs of hematite photoanodes prepared with spin coating precursor sol solutions containing either (g) 0, (h) 0.05, (i) 0.15 ml of 37% HCl. The micrograph for 0.10 ml of 37% HCl is Figure 1a.

Spin coating and heat treatment resulted in photoanodes of high optical quality suitable for photocurrent measurements under simulated sunlight. The addition of PVC-*g*-POEM graft copolymer was crucial to obtain worm-like porosity (Figure 1). In absence of polymer, spin coating hematite precursor suspensions were of low viscosity and resulting films were dense and of poor photoelectrochemical performance (Figure S3). It indicates that the PVC-g-POEM graft copolymer played a pivotal role in controlling the structure, morphology and photoelectrochemical performance of electrode. Since an optimized single layer was of low thickness, multilayer hematite photoanodes were prepared and comparison of structure and performance made. Multilayers were formed by depositing additional layers by spin-coating and heating up to 800 °C using the three step sintering process for each layer prior to deposition of the next layer. Photographs of resulting hematite photoanodes on FTO-ABS supports with one, two, and three hematite layers are shown in Figure 2a. Opacity of the slides increased with increasing layer number. Morphology of the upper surfaces is shown in Figure 1a-c, analyzed by FE-SEM. Surface coverage and analyzed particle size are shown in Table 1. The average particle size increases from 65 to 69 and 72 nm, for one, two and three layers, respectively. For one layer, there are plenty of void spaces, which are filled with the second layer deposition (Figure 1a-b). With the third layer, there are again many empty void spaces (Figure 1c). Corresponding cross-sectional SEM micrographs are shown in Figure 1d-f. Photoanodes consisted of the following multilayer stack (from the bottom to the top in FE-SEM micrographs): ABS glass support, FTO of approx. 500 nm, and hematite, as also depicted in Scheme 1b. Cross-sectional micrographs show hematite films prepared with either one or two layers had similar thickness around 280 nm (± 20nm), since the second deposition process mainly filled the vacant areas within the hematite first layer film (Figure 1a-b). Some islands are present above the height of the first layer, but not homogeneously distributed (note the material out of focus on the top right side of Figure 1e). Upon the deposition of a third layer, the thickness increased to approximately 400 nm (± 20nm) in

total showing that once vacant areas were filled a further overlying layer of hematite was formed. These results also indicate the possibility that once the FTO is covered with hematite, the wetting changes and then less material is deposited per deposition cycle. These measurements were repeated three times to check reproducibility. When their photoresponse was tested, the photoanode prepared with only one-layer deposition showed the best performance for both forward and backward illumination due to their smaller particle size (Figure 2b). Therefore, it can be concluded that multilayer deposition resulted in denser and thicker hematite layers that was detrimental to generated photocurrent.
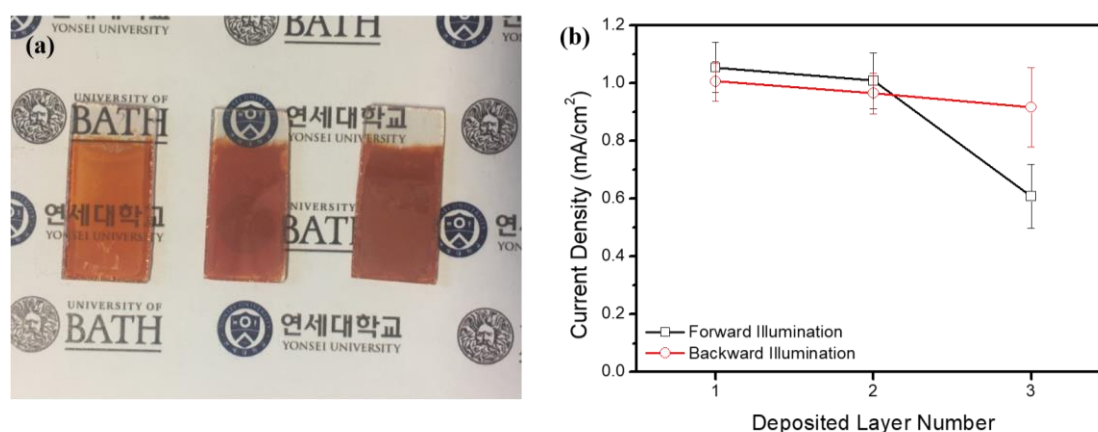
Figure 2. (a) Photograph of hematite photoanodes prepared with either one, two or three layers (from left to right) and (b) their photocurrent density measurements at 1.23 V_{RHE} under 100 mW cm^{-2} AM1.5G solar illumination. Spin coating precursor sol solutions were prepared with 0.1 ml of 37% HCl.

Table 1. Preparation conditions of sol solutions for spin coating deposition, final particle size and surface coverage in sintered hematite photoanodes, and photocurrent densities measured at 1.23 V_{RHE} under 1 sun AM1.5 illumination in aqueous KOH.

Sample Name	Polymer Concentration [wt %][a]	Acac-hematite [mg][b]	37% HCl [mL]	Number of Depositions	Film Particle Size [nm]	Surface Coverage [%]	Photocurrent Density [mAcm^{-2}] (Forward/Backward)
0.00ml HCl	6.0	30	0	1	73 ± 25	46	0.72 ± 0.18 / 0.78 ± 0.04
0.05ml HCl	6.0	30	0.050	1	73 ± 15	58	0.84 ± 0.08 /

							0.93 ± 0.05
0.10ml HCl	6.0	30	0.100	1	67 ± 19	65	1.05 ± 0.09 / 1.01 ± 0.07
0.10ml HCl-2L	6.0	30	0.100	2	75 ± 14	69	1.01 ± 0.10 / 0.96 ± 0.07
0.10ml HCl-3L	6.0	30	0.100	3	78 ± 13	72	0.61 ± 0.11 / 0.92 ± 0.14
0.15ml HCl	6.0	30	0.150	1	84 ± 16	61	0.50 ± 0.22 / 0.60 ± 0.25

a) wt% (polymer weight % in THF); (b) Hematite coated with acac; L -Multilayer deposition

3.3 Addition of hydrochloric acid to hematite precursor sol solutions

The effect of adding HCl acid to the sol solution containing the hematite nanoparticles for spin coating was examined. 0.05, 0.1, or 0.15 ml of aqueous 37% HCl was added to the prepared sol solutions and stirred overnight. A sample without acid was also prepared (see Experimental Section). Spin coating deposition and heating at 200, 500 and 800 °C resulted in films of different morphology and performance for the different amounts of HCl added (Table 1). SEM micrographs of the top surfaces of this series are shown in Figure 1g-i. With no HCl, patches of FTO were visible alongside the hematite coating (Figure 1g). Increasing the level of HCl up to 0.1ml resulted in improved hematite coating in terms of uniformity and reduced particle size (Figure 1h and 1a). At higher acid content (0.15 ml) miscibility of polymer and solvent became poor and hematite coatings became more disordered with large cracks visible (Figure 1i and S4).

Surface OH groups on final hematite films (after the heating steps) were characterized by X-ray photoelectron spectroscopy (XPS). In Figure 3a, the XPS O 1s spectra show characteristic binding energy peaks: a quite sharp peak at 529.2 eV, attributed to Fe-O in the hematite lattice, and a broad peak at 530.9 eV, attributed to adsorbed atomic oxygen [35,36]. With HCl addition to the sol solutions, a large peak at 529.3 eV was obtained corresponding to surface Fe-OH [36]. Surface levels of Sn were observed (Table S1) because the Sn ions in FTO can diffuse to the electrode at high temperatures such as 800 °C during the calcination, which improves hematite conductivity at a low content of Sn [35-37]. In particular, the Sn content was lowest for the 0.10 ml HCl electrode with the

highest performance, indicating the measured concentration of Sn ions is not a critical parameter. The high photocurrent density of 0.10 ml HCl electrode is due to the uniform hematite coating and absence of cracks revealing the FTO coating layer. The XPS results indicated that the amount of HCl added affects the formation of surface OH groups, which can enhance photocurrent density due to surface passivation [37].

FT-IR spectroscopy on sol solutions that were vacuum-dried was also employed to study the addition of HCl acid. Absorption shifts of the ether C-O bond (from 1110 to 1077 cm^{-1}) and ester C=O bond (from 1728 to 1721 cm^{-1}) are observed with the addition of HCl (Figure 3b-c). This indicates an interaction between the iron oxide nanoparticles and POEM copolymer side chains. Moreover, dried solution of the 0.1mlHCl sample gave IR broad bands at 3200 and 1650 cm^{-1} consistent with stretching and bending of water adsorbed on FeOOH hydroxyls [38,39]. These vibrations were minimal in the films prepared in the absence of HCl. Powder XRD of the dried 0.1mlHCl sample gave reflections due to the hematite and additional small peaks that matched to FeOOH akaganeite and lepidrocrocite strongest reflections (Figure 3d). These results demonstrate that hematite leaching by HCl in the sol solutions produces FeOOH akaganeite and lepidrocrocite particles which interact with POEM side chains in PVC-*g*-POEM, eventually forming a wormlike mesoporous structure upon heating.
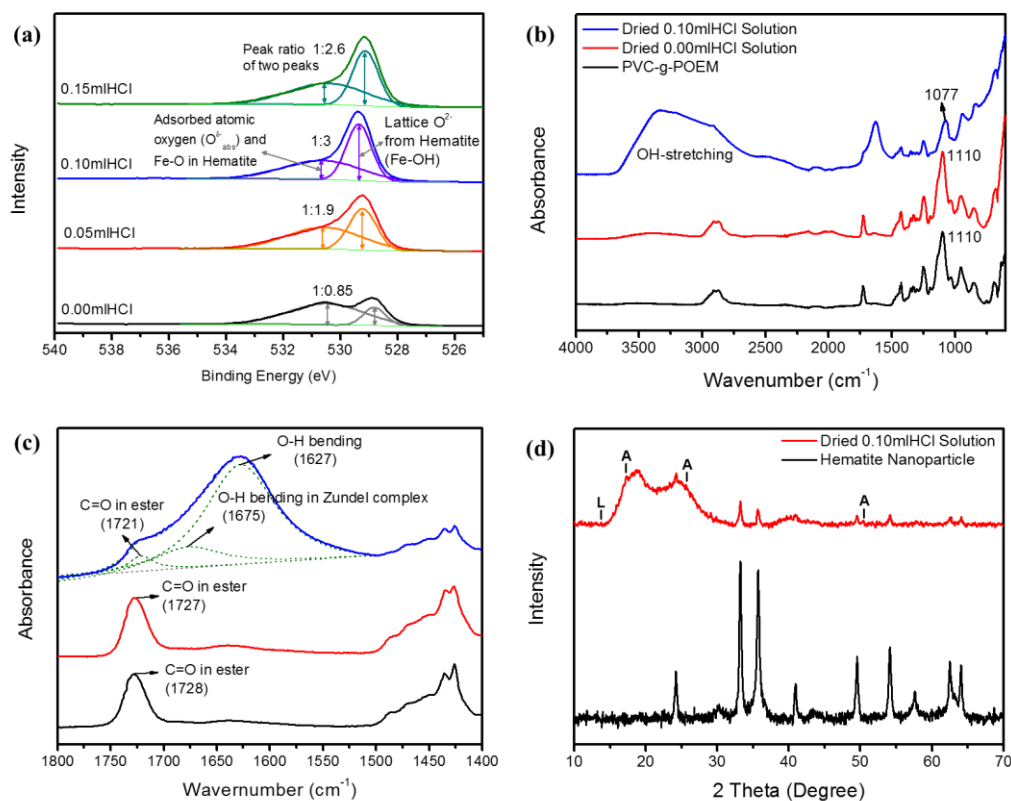
Figure 3. (a) Oxygen XPS analysis of hematite photoanodes prepared with spin coating precursor sol solutions containing different amounts of aqueous 37% HCl. (b) FT-IR spectra of dried spin coating precursor sol solutions prepared with either 0.0 or 0.10 ml of 37% HCl and spectrum of PVC-*g*-POEM copolymer. (c) Magnified previous IR spectra showing red shift of C=O stretching region for sols containing HCl. (d) Powder XRD of dried sol solution prepared with 0.10 ml of 37% HCl, showing reflections due to α-Fe_2O_3 hematite and FeOOH as akaganeite (A) and lepidocrocite (L) as compared to hematite starting material.
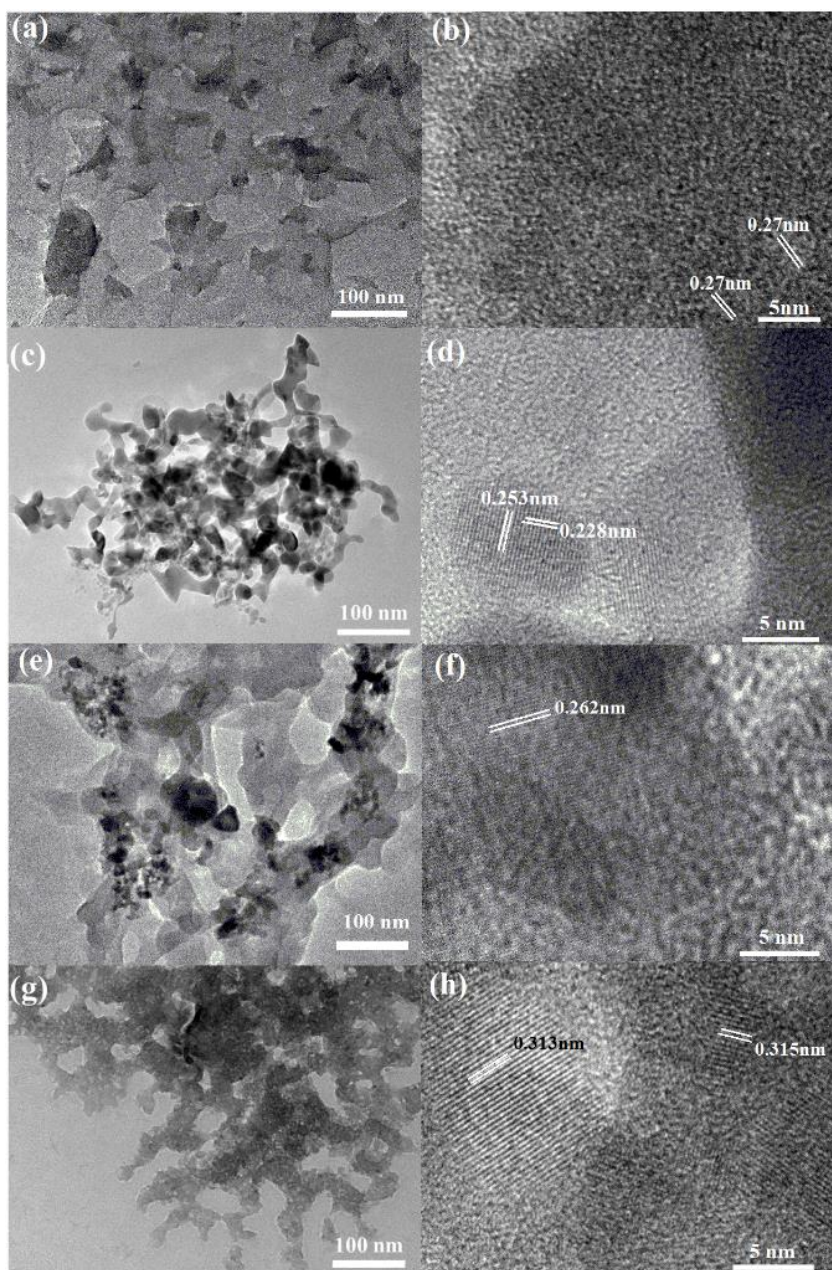
Figure 4. TEM micrographs of air dried spin coating precursor sol solutions prepared with (a,b) 0, (c.d) 0.05, (e.f) 0.10, and (g,h) 0.15 ml of 37% HCl. Measured lattice spacings are shown.

TEM observation of vacuum-dried (uncalcined) sol solutions, containing hematite-acac and PVC-*g*-POEM graft copolymer (no HCl), showed the presence of polymer and 10nm hematite starting material (Figure 4a-b). A lattice spacing of dÅ=2.70 corresponding to the (104) plane of

hematite is shown (Figure 4b). After inclusion of HCl into the sol solution TEM of the 0.05mlHCl sample showed lattice spacings corresponding to the dÅ = 2.53 and 2.28, (112) and (013) planes resp., of β-FeOOH akaganeite (Figure 4c-d). For 0.1 ml HCl addition, a dÅ = 2.62 (004) lattice spacing corresponding to β-FeOOH akaganeite was also observed (Figure 4e-f). For 0.15 ml HCl addition, particle sizes were reduced down to 5 nm with observable lattice spacings corresponding to dÅ = 3.13 (400) γ-FeOOH lepidrocrocite (Figure 4g-h). These TEM results further confirm the FTIR and XRD characterization and reveals the degree of conversion the hematite precursor nanoparticles are exposed to in the sol solutions with THF, acac, PVC-g-POEM and aqueous concentrated HCl. In addition, the TEM showed the hematite/FeOOH clusters to be well dispersed throughout the copolymer, attributed to the selective interaction between POEM side chains and α-Fe$_2$O$_3$/FeOOH nanoparticles. Finally, TEM showed the presence of micelle structures with low electron density zones due to POEM side chains and higher electron density regions due to PVC main chains in the background of Figure 4e [29].

HCl effects were also reflected in the color of the sols. In absence of acid or with 0.05 ml HCl addition the sols were orange-red. This altered to yellow-orange with 0.1 ml HCl addition. Finally, with 0.15 ml HCl addition, a yellow sol was obtained. The changes in color are attributed to the different phases formed and resulting particle sizes. α-Fe$_2$O$_3$ hematite is known to be red and both β-FeOOH akaganeite and γ-FeOOH lepidrocrocite yellow/brown [40]. Therefore, the changes in color further confirmed FT-IR and TEM observations, indicating HCl addition results into dissolution and reprecipitation of hematite nanoparticles into akaganeite and lepidrocrocite with the assistance of THF, acac, and PVC-g-POEM graft copolymer.

Overall, the characterization suggests that HCl treatment of hematite nanoparticles in the presence of the copolymer resulted in dissolution – reprecipitation processes at the surface of the

hematite starting material and the formation of mixed iron oxide hydroxides. These iron oxide hydroxides interact with POEM side chains, allowing a better dispersion of particles in the sol solutions containing the copolymer micelles.

3.4 Photoelectrochemical performance

The photocurrent density performances of hematite photoanodes prepared with different amounts of HCl were measured at 1.23 V_{RHE} under 1 sun illumination (100 mW cm^{-2}, with an AM1.5G filter, Figure 5a). It was found that thermal annealing at 800 °C did not significantly affect the conductivity of FTO (10 ohm/sq.), indicating negligible effect of the Sn diffusion on the electrical properties of FTO. All the photoanodes prepared presented positive and negative photocurrent spikes. The positive photocurrent spikes in hematite photoanodes have been assigned to accumulation of holes in the semiconductor space charge region under illumination, whereas the negative ones upon turning of the illumination are associated with recombination of bulk electrons with holes accumulated in the space charge region during irradiation [41]. The best performance was obtained with the 0.10ml HCl samples, reaching a photocurrent of 1.05 ± 0.09 mA cm^{-2} at $1V_{RHE}$. Little difference between forward and backward illumination was obtained, indicating no excessive thickness and good percolation of the electrolyte in the porous hematite film (Figure 5b) [42]. The performance trend can be matched to that of particle size and nature of surface coverage on 0, 0.05 and 0.10 ml HCl samples. Nanoparticle dimension helps to mitigate against the short hole diffusion length of hematite, accordingly the smallest sized 0.10mlHCl sample exhibited best performance. The 0.15mlHCl sample exhibited low performance and large deviation in photocurrent density owing to macro-scale and micro-scale film cracks (Figure S4). These cracks formed upon sintering must result from the shrinkage of the film constrained by the substrate, giving rise to stresses [43]. They strongly depend on the pre-sintering

microstructure of the film and density. Since 0.15 ml of HCl addition resulted in complete

dissolution of hematite nanoparticles and transformation to smaller FeOOH nanoparticles, spin

coated films must have been more susceptible to stresses during the sintering. This indicates there is

a limit for HCl addition, above which the effects can be counterproductive for the quality of the films.

A preliminary stability test for the best performing photoanode (0.10ml HCl sample) was conducted

for 10 repeated intervals of continuous illumination for 3 min (Figure 5c). During the 3-min

illumination intervals, the photocurrent density steadily decreased by 6.0%. After turning on the

illumination, the photocurrent density returned to the last value, indicating degradation only occurs

during illumination. After 10 intervals (i.e. 30 min of total irradiation), a photocurrent density of

93.9 % was preserved, indicating the hematite coating was of high stability.
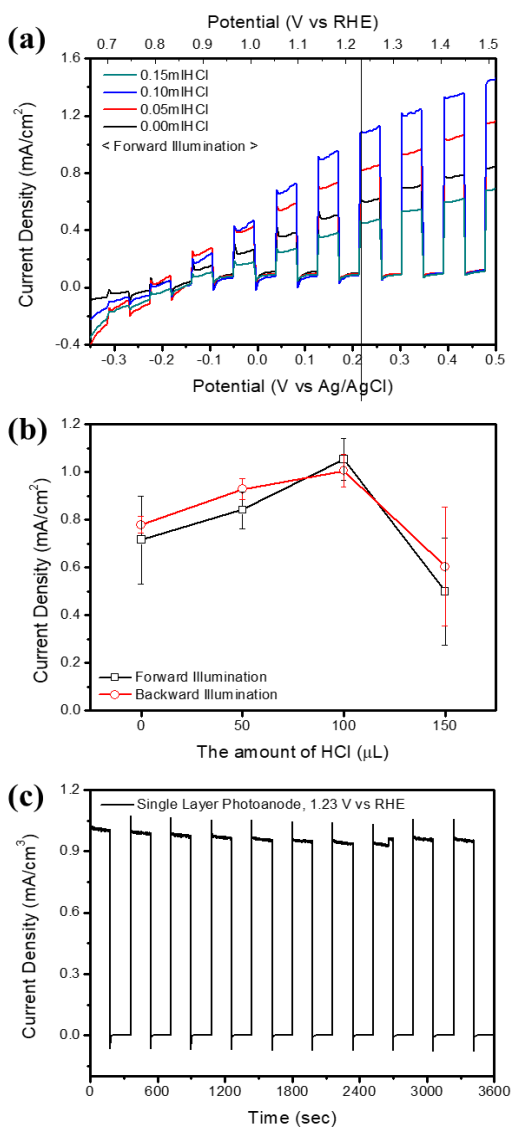
Figure 5. Photoelectrochemical results of hematite photoanodes prepared with spin coating precursor sol solutions with different amounts of HCl. (a) Representative current densities under chopped forward light. (b) Current densities at 1.23 V_{RHE} with either forward or backward illumination. (c) Stability test of a hematite photoanode prepared with 0.1 ml of 37% HCl with light chopped in 3min ON - 3min OFF intervals. Measurements were done with 1 sun illumination (100mW cm-2, AM1.5G filtered) in 1 M KOH.
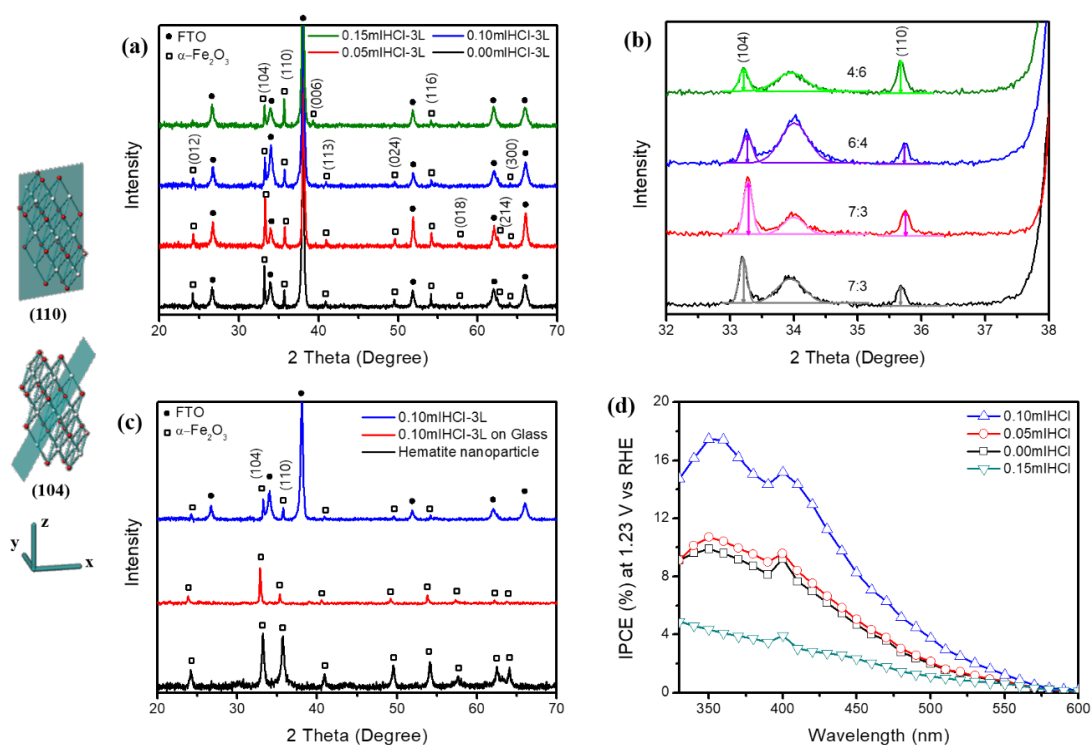
Figure 6. (a) XRD pattern of hematite photoanodes with a total of three layers deposited by repeating spin coating and heating cycles three times. Spin coating precursor sol solutions were prepared with different amounts of aqueous 37% HCl. (b) Previous XRD patterns magnified to compare (104) and (110) intensities. (104):(110) ratios are calculated and presented on charts. (c) XRD patterns of starting ~10 nm hematite particles and resulting hematite 3-layer films deposited either on FTO-coated ABS glass or simply ABS glass. (d) IPCE spectra of hematite photoanodes prepared with spin coating precursor sol solutions containing different amounts of aqueous 37% HCl.

The photoanodes with only one deposited layer were found to be too thin to observe clear XRD characteristic peaks. A total of three layers were instead laid down repeating deposition and heating cycles to have enough thickness for XRD. Figure 6a shows the XRD pattern of the photoanodes, with diffraction peaks assigned to FTO and α-Fe$_2$O$_3$ hematite. The XRD peaks at 33.2° and 35.7° of 2 theta (°) correspond to the (104) and (110) planes, respectively. Their intensity is similar (a ratio of 1.06:1) in randomly oriented hematite (JCPDS-33-664). Patterns show that the three layers prepared from sol solutions containing increasing

HCl resulted in increased intensity of the (110) plane relative to (104) one (Figure 6b). It changed from a (104):(110) ratio of 7:3 for 0 and 0.05ml HCl samples to 6:4 and 4:6 for 0.10 and 0.15 ml HCl samples, respectively. This was most likely due to increased dissolution of hematite starting material and reprecipitation into iron oxide hydroxides, which must have a different sintering behavior. When a hematite photoanode was fabricated on an ABS glass substrate (without FTO coating), the hematite (104):(110) ratio was higher (5:1 vs. 6:4, Figure 6c). Therefore, it can be concluded that both the FTO glass and HCl play a pivotal role in enhancement of the (110) plane. Promoting the (110) crystal orientation over the (104) is important for a higher electron transport and photoresponse, as previously demonstrated on thin hematite films grown solely in either directions [44].

Light absorption properties and band gap energies of hematite photoanodes were studied by incident photon-to-current efficiency (IPCE) and ultraviolet–visible (UV-vis) spectra (Figure 6d and S5). The IPCE efficiency was consistent with photocurrent density results, with the 0.10mlHCl sample giving the highest efficiency of ~15% at the visible / UV light boundary. All samples showed characteristic UV-vis absorption regions of hematite [37], with an absorption edge corresponding to a band gap around 2-2.1 eV and no dependence on the HCl amount used (Figure S5).

Post-synthesis acid treatment of hematite photoanodes have recently been shown to help suppress the electron-hole recombination [37]. The post-synthesis acid treatment with HCl or other acids increases the amount of hydroxyl functional groups at the hematite surface which passivates surface electron traps and improves the efficiency of charge separation. This work reveals that similar results can be obtained without a post-synthesis extra step. Addition of acid to the spin coating precursor sol solution has similar effects in increasing the amounts of surface hydroxyls leading to surface passivation.

HCl has been previously used to manipulate hematite layer thickness in a hydrothermal synthesis [44]. We have shown here that HCl can also be used to transform the surface of hematite particles into FeOOH phases. This dissolution and reprecipitation results in smaller and more interactive nanoparticles and clearer sol solutions with better qualities for spin coating deposition. This is encouraging, since spin coating of non-clear nanoparticle suspensions often create films with defects such as striations and comets. In those cases, doctor blading deposition is used instead, but it is less reproducible and user-friendly than spin coating deposition.

Due to the intrinsic limitations of bare hematite such as poor charge carrier mobility and short hole diffusion length, the preparation method strongly influences the final anodic photocurrents in the absence of co-deposited electrocatalysts. One of highest photocurrents for bare hematite have been obtained by (expensive) atmospheric pressure chemical vapor deposition, with values close to 2 mA cm^{-2} at 1.23 V$_{RHE}$ [45]. Less expensive solution processes involving doctor blading obtain lower photocurrents, with values for bare hematite typically below 1 mA cm^{-2} at 1.23 V$_{RHE}$ [42,46]. Solution processes consisting of direct solvothermal crystal growth of hematite precursors on immersed FTO-coated glass obtains higher anodic photocurrents with best values slightly above 1 mA cm^{-2} at 1.23 V$_{RHE}$ but they have difficulties for scale up [27,47]. This facile and economical solution process method using an amphiphilic graft copolymer, commercial hematite nanoparticles, HCl addition, and spin coating deposition reaches 1.05 ± 0.09 mA cm^{-2} at 1.23 V$_{RHE}$ for optimal samples, very competitive values compared to the current state of the art.

4. Conclusions

Novel wormlike mesoporous hematite films were prepared by spin coating deposition and calcination using as spin coating precursors sol solutions prepared with an amphiphilic PVC-*g*-

POEM graft copolymer, commercially available ~ 10 nm hematite nanoparticles, acac, aqueous HCl and THF solvent. The graft copolymer, used for the first time with hematite, was very effective in adding porosity and limiting particle size in final hematite films. Particles in hematite films were typically below 100 nm diameter and best results were obtained for 65 nm dimension particles and ~280 nm thickness. HCl was also found crucial for generating final properties and optimizing performance of hematite films. Its addition to the sol solutions resulted in the outer surface or complete dissolution of the ~ 10 nm hematite nanoparticles, with re-precipitation of either a surface layer of mixed γ-FeOOH and β-FeOOH or complete conversion to 5 nm-sized β-FeOOH. Analysis indicated the hydrophilic rubbery POEM chains of the graft copolymer interacted with the FeOOH, assisting HCl in this dissolution, which also helped to achieve clearer sol solutions easier to spin coat. Eventually, heat treatment at 200, 500 and 800 °C of spin coated films converted materials back to α-Fe_2O_3 hematite and sintered the films achieving films of high optical quality. The initial conversion of α-Fe_2O_3 hematite to FeOOH was found beneficial for two purposes. First, it influenced the final crystal orientation in hematite films, enhancing the (100) plane which is associated with raised photocurrent performance. Second, it increased the amount of hydroxyl functional groups on final hematite films which have a role in reducing electron recombination due to their passivation effect. Overall, optimized hematite photoanodes achieved 1.05 ± 0.09 mA cm^{-2} at 1.23 V_{RHE} of photocurrent density when illuminated with solar simulated light. A preliminary stability test for a total of 30 min illumination resulted in only a decrease to 93.9 % of photocurrent density, showing high stability. To conclude, a facile, economical, effective and novel fabrication approach for hematite photoanodes is here presented using commercially available materials and inexpensive solution process techniques. Further studies on increasing photocurrent by surface metal loading are currently underway to leverage their high porosity and ease of preparation.

5. Acknowledgements

All data created during thisresearch are openly available from the University of Bath data archiveat DOI number 10.15125/BATH-00467.

References

[1] H. S. Han, S. Shin, D. H. Kim, I. J. Park, J. S. Kim, P.-S. Huang, J. K. Lee, I. S. Cho, X. Zheng, Energy Environ. Sci., 11 (2018) 1299-1306.

[2] J. Zhao, T. M. Gill, X. Zheng, Nano Research, 11 (2018) 3499–3508.

[3] X. Xia, S. Peng, Y. Bao, Y. Wang, B. Lei, Z. Wang, Z. Huang, Y. Gao, Journal of Power Sources, 376 (2018) 11-17.

[4] R. Zhang, M. Shao, S. Xu, F. Ning, L. Zhou, M. Wei, Nano Energy 33 (2017) 21-28.

[5] D. E. Schipper, Z. Zhao, A. P. Leitner, L. Xie, F. Qin, M. K. Alam, S. Chen, D. Wang, Z. Ren, Z. Wang, J. Bao, K. H. Whitmire, ACS Nano 11 (2017) 4051-4059.

[6] X. Xu, Z. Bao, W. Tang, H. Wu, J. Pan, J. Hu and H. Zeng, Carbon 121 (2017) 201-208.

[7] K. Sivula, R. Zboril, F. Le Formal, R. Robert, A. Weidenkaff, J. Tucek, J. Frydrych, M. Grätzel, J. Am. Chem. Soc. 132 (2010) 7436-7444.

[8] P. Kuang, L. Zhang, B. Cheng, J. Yu, Appl. Catal. B-Environ. 218 (2017) 570-580.

[9] T. H. Jeon, G.-h Moon, H. Park, W. Choi, Nano Energy 39 (2017) 211-218.

[10] J. Wang, J. L. Waters, P. Kung, S. M. Kim, J. T. Kelly, L. E. McNamara, N. I. Hammer, B. C. Pemberton, R. H. Schmehl, A. Gupta, S. Pan, ACS Appl. Mater. Interfaces 9 (2017) 381-390.

[11] A. Kafizas, L. Francàs, C. Sotelo-Vazquez, M. Ling, Y. Li, E. Glover, L. McCafferty, C. Blackman, J. Darr, I. Parkin, J. Phys. Chem. C 121 (2017) 5983-5993.

[12] Y. Liu, J. Li, W. Li, Y. Yang, Y. Li, Q. Chen, J. Phys. Chem. C 119 (2015) 14834-14842.

[13] J. Zhang, I. Salles, S. Pering, P. J. Cameron, D. Mattia, S. Eslava, RSC Adv. 7 (2017) 35221-35227.

[14] P. Dias, A. Vilanova, T. Lopes, L. Andrade, A. Mendes, Nano Energy 23 (2016) 70-79.

[15] Y. Ling, G. Wang, H. Wang, Y. Yang, Y. Li, ChemSusChem 7 (2014) 848-853.

[16] A. Kay, I. Cesar, M. Grätzel, J. Am. Chem. Soc. 128 (2006) 15714-15721.

[17] Y. Ling, G. Wang, J. Reddy, C. Wang, J. Z. Zhang, Y. Li, Angew. Chem.-Int. Edit. 51 (2012) 4074-4079.

[18] S. Shen, S. A. Lindley, X. Chen, J. Z. Zhang, Energy Environ. Sci. 9 (2016) 2744-2775.

[19] A. G. Tamirat, J. Rick, A. A. Dubale, W.-N. Su, B.-J. Hwang, Nanoscale Horiz. 1 (2016) 243-267.

[20] K. Itoh, J. O. M. Bockris, J. Electrochem. Soc. 131 (1984) 1266-1271.

[21] A. J. Bosman, H. J. van Daal, Adv. Phys. 19 (1970) 1-117.

[22] F. Le Formal, S. R. Pendlebury, M. Cornuz, S. D. Tilley, M. Grätzel, J. R. Durrant, J. Am. Chem. Soc. 136 (2014) 2564-2574.

[23] M. Barroso, S. R. Pendlebury, A. J. Cowan, J. R. Durrant, Chem. Sci. 4 (2013) 2724-2734.

[24] J. H. Kennedy, K. W. Frese, J. Electrochem. Soc. 125 (1978) 709-714.

[25] R. H. Gonçalves, B. H. R. Lima, E. R. Leite, J. Am. Chem. Soc. 133 (2011) 6012-6019.

[26] W. Hamd, S. Cobo, J. Fize, G. Baldinozzi, W. Schwartz, M. Reymermier, A. Pereira, M.

Fontecave, V. Artero, C. Laberty-Robert, C. Sanchez, Phys. Chem. Chem. Phys. 14 (2012) 13224-13232.

[27] J. Y. Kim, G. Magesh, D. H. Youn, J.-W. Jang, J. Kubota, K. Domen, J. S. Lee, Sci. Rep. 3 (2013) 2681.

[28] S. Kment, P. Schmuki, Z. Hubicka, L. Machala, R. Kirchgeorg, N. Liu, L. Wang, K. Lee, J. Olejnicek, M. Cada, I. Gregora, R. Zboril, ACS Nano 9 (2015) 7113-7123.

[29] S. H. Ahn, J. H. Koh, J. A. Seo, J. H. Kim, Chem. Commun. 46 (2010) 1935-1937.

[30] S. H. Ahn, W. S. Chi, J. T. Park, J. K. Koh, D. K. Roh, J. H. Kim, Adv. Mater. 24 (2012) 519-522.

[31] J. T. Park, S. H. Ahn, D. K. Roh, C. S. Lee, J. H. Kim, ChemSusChem 7 (2014) 2037-2047.

[32] D. J. Kim, J. K. Kim, J. H. Lee, H. H. Cho, Y.-S. Bae, J. H. Kim, J. Mater. Chem. A 4 (2016) 12497-12503.

[33] D. K. Roh, S. J. Kim, H. Jeon, J. H. Kim, ACS Appl. Mater. Interfaces 5 (2013) 6615-6621.

[34] M. M. Nasef, E.-S. A. Hegazy, Prog. Polym. Sci. 29 (2004) 499-561.

[35] A. P. Grosvenor, B. A. Kobe, N. S. McIntyre, Surf. Sci. 572 (2004) 217-227.

[36] J. Baltrusaitis, D. M. Cwiertny, V. H. Grassian, Phys. Chem. Chem. Phys. 9 (2007) 5542-5554.

[37] Y. Yang, M. Forster, Y. Ling, G. Wang, T. Zhai, Y. Tong, A. J. Cowan, Y. Li, Angew. Chem. 128 (2016) 3464-3468.

[38] S. Kang, G. Wang, M. Fang, H. Wang, X. Wang, W. Cai, J. Mater. Res. 30 (2015) 1629-1638.

[39] M. Thämer, L. De Marco, K. Ramasesha, A. Mandal, A. Tokmakoff, Science 350 (2015) 78-82.

[40] R. A. Antunes, I. Costa, D. L. A. D. Faria, Mater. Res. 6 (2003) 403-408.

[41] A. G. Tamirat, A. A. Dubale, W.-N. Su, H.-M. Chena, B.-J. Hwang, Phys. Chem. Chem. Phys. 19 (2017) 20881-20890.

[42] O. S. Hammond, S. Eslava, A. J. Smith, J. Zhang, K. J. Edler, J. Mater. Chem. A 5 (2017)

16189-16199.

[43] F. Li, J. Pan, A. Cocks, J. Am. Ceram. Soc. 95 (2012) 3743-3749.

[44] A. Pu, J. Deng, Y. Hao, X. Sun, J. Zhong, Appl. Surf. Sci. 320 (2014) 213-217.

[45] D. K. Zhong, M. Cornuz, K. Sivula, M. Gratzel, D. R. Gamelin, Energy Environ. Sci. 4 (2011) 1759-1764.

[46] J. Brillet, M. Grätzel, K. Sivula, Nano Lett. 10 (2010) 4155-4160.

[47] J. Y. Kim, D. H. Youn, J. H. Kim, H. G. Kim, J. S. Lee, ACS Appl. Mater. Interfaces 7 (2015) 14123-14129.